ACSNANO

www.acsnano.org

Electrospray Deposition of PbSe Quantum Dot Superlattices with Improved Uniformity and Structural Perfection

Geemin Kim, Cristian Reynaga Gonzalez, and Matt Law*

Cite This: https://doi.org/10.1021/acsnano.6c01980

Read Online

ACCESS | Metrics & More | Article Recommendations | Supporting Information

ABSTRACT: Colloidal PbX (X = Se, S) quantum dots (QDs) can be self-assembled into highly ordered three-dimensional superlattice (SL) films and subsequently fused by ligand exchange to produce epitaxially interconnected SLs (epi-SLs) with strong inter-QD electronic coupling and the potential for fully delocalized electronic states. However, the conventional method of fabricating these films by drop casting a QD dispersion onto the surface of liquid ethylene glycol (EG) suffers from uncontrolled lateral liquid flows during spreading and drying that result in nonuniform, irreproducible SL films with substantial flow-induced QD positional disorder (riverlike flow patterns in the QD chains). Here, we use electrospray deposition (ESD) to make PbSe QD SL films on EG that are uniform over large areas (~20 cm^2) and have much less QD positional disorder compared to drop-cast SL films. The suppression of flow-induced structural disorder in ESD films is attributed to the unique ability of ESD to deposit a microscopically thin layer of QD dispersion that slowly dries in place without macroscopic liquid flow. SL film thickness is readily tuned by changing the sprayed volume. Moreover, epi-SLs made from ESD films have better positional order than epi-SLs made from drop-cast films. ESD enables the reproducible fabrication of 3D PbSe QD epi-SLs of excellent uniformity and structural quality for studying miniband transport and other collective electronic phenomena. Fabrication of films of CdSe QDs and $ZnFe_2O_4$ nanocrystals on EG shows that ESD is a general method for making high-quality, large-area nanocrystal films of uniform and controlled thickness for a variety of applications.

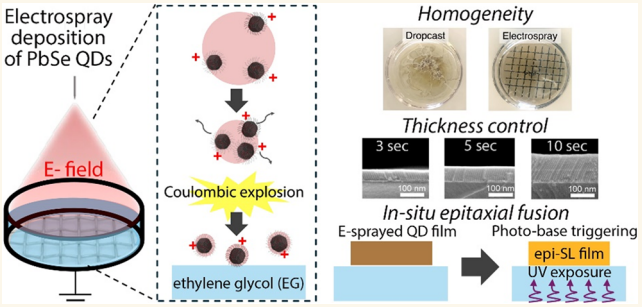

KEYWORDS: *colloidal quantum dots, electrospray deposition, superlattice, PbSe, structural characterization, disorder*

INTRODUCTION

Epitaxially fused quantum dot (QD) superlattices (epi-SLs)—crystals of epitaxially interconnected colloidal QDs—combine extraordinary spatial order with strong inter-QD electronic coupling and are predicted to feature electronic minibands that enable high-mobility, bandlike charge transport.[1−13] PbX (X = Se, S) QD epi-SL films are typically made by self-assembly and ligand exchange on a liquid surface followed by stamp transfer to a solid substrate (the Langmuir−Schaefer technique). In this process, a SL film of monodisperse, oleate-capped PbX QDs is first self-assembled on the surface of a liquid substrate, which is usually ethylene glycol (EG).[14−16] Next, the floating oleate-capped SL is converted to an epi-SL by a chemical or thermal treatment that removes oleate from the QD surface, resulting in SL densification and the oriented attachment (necking or partial fusion) of adjacent QDs across their {100} facets.[7,9,11,17,18] The epi-SL film is then stamp transferred to a solid substrate (e.g., silicon), where it may undergo additional treatments such as infilling with a metal oxide by atomic layer deposition (ALD) to enhance its energetic order, charge carrier mobility, and operational stability.[13,19−21]

We previously reported the fabrication of high-quality multilayer (3D) PbSe QD epi-SL films up to 250 nm thick, established their structure (the complete superlattice unit cell) using X-ray scattering and correlative electron microscopy and diffraction of single SL grains, and determined how they form from the parent oleate-capped SL.[11] We showed that the oleate-capped SL adopts a rhombohedrally distorted body-centered cubic unit cell in which each QD is surrounded by six nearest neighbors that are rotationally aligned in 3D with

Received: January 31, 2026
Revised: July 2, 2026
Accepted: July 6, 2026

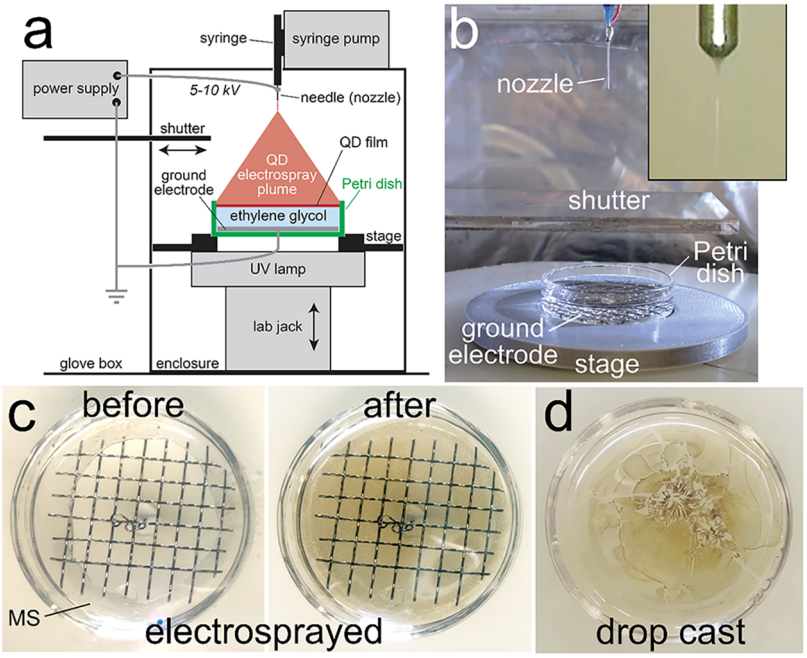

Figure 1. Electrospray deposition of PbSe QD superlattice films onto the surface of ethylene glycol. (a) Schematic of the ESD system used in this work. The system is housed in an N_2-filled glovebox. (b) Photograph of the interior of the ESD enclosure showing the nozzle, grounded quartz Petri dish containing EG, and movable plastic shutter. Inset is a photograph of the nozzle, electrospray cone jet, and plume during ESD of a 60 mg/mL dispersion of 7.1 nm oleate-capped PbSe QDs in decane (applied bias = 8.4 kV; nozzle-to-EG distance = 8 cm; flow rate = 0.05 mL/min). The outer diameter of the nozzle is 0.74 mm. A video showing ESD of a PbSe QD film is presented in the Supporting Information (Video S1). Close-up videos of the nozzle under various operating conditions are also provided (Videos S3, S4, S5 and S6). (c) Plan-view images from Video S1 showing the quartz Petri dish before (*left*) and after (*right*) ESD of a 60 mg/mL dispersion of 7.1 nm QDs in decane at a flow rate of 0.09 mL/min for 5 s (total sprayed volume = 7.5 μL). The floating QD film has a uniform brown color and is 70 nm thick. The outer diameter of the Petri dish is 2 in. A stainless steel wire cloth ground electrode sits at the bottom of the Petri dish approximately 5 mm under the EG surface and is connected to the power supply via a stainless steel wire threaded through a hole drilled through the center of the Petri dish and then sealed with epoxy. A plastic meniscus shield (MS) placed on top of the dish in the left image was removed after film deposition to facilitate uniform drying of the film (right image). (d) Image of a typical QD film made by drop casting (10 mg/mL dispersion of 7.1 nm QDs in hexane, total deposited volume = 90 μL). The film is highly nonuniform. See Video S2 for the corresponding video of the fabrication of this drop-cast film.

cofacial {100} facets. This arrangement prepositions the QDs for facile epitaxial fusion of their {100} facets to form a distorted simple cubic epi-SL with excellent spatial order in three dimensions. The phase transition from the oleate-capped SL to the epi-SL occurs by translational motion and only a slight rotation (~10°) of each QD, avoiding the need for large coordinated QD rotations that would increase spatial disorder and defects. This phase transition combines "distributed" epitaxy (i.e., coordinated epitaxial necking of ~10^{18} QDs cm^{-3} in 3D) with atomic topotaxy (i.e., the atomic lattices of the parent and product SLs have a specific 3D crystallographic relationship). The structural perfection of the epi-SL is determined by the perfection of its parent oleate-capped SL and the dynamics of the phase transition from the oleate-capped SL to the epi-SL.

The structural perfection of state-of-the-art oleate-capped SLs can be greatly improved. These SLs are normally prepared by drop casting and slowly drying a dispersion of oleate-capped QDs in a volatile nonpolar solvent (e.g., hexane) on EG. However, upon drop casting, the QD dispersion spreads across the EG surface in a complex, turbulent, and irreproducible fashion, causing two main problems. First, macroscopic liquid flows during drying create lateral flow patterns in the films—riverlike meanders, arcs, and swirls of the QD chains within the SL grains. Such flow-induced QD positional disorder is believed to produce missing necks, neck polydispersity, QD positional and orientational misalignment, nanoscale rips, and reduced grain size in the resulting epi-SLs. Second, the haphazard bulk liquid flow results in heterogeneous, often discontinuous films of nonuniform thickness and possessing a high density of bare regions, cracks, and other macroscopic defects. Drop-cast films are not reproducible. Since the uniformity and structural perfection of an epi-SL cannot exceed that of its parent oleate-capped SL, it is important to develop fabrication methods for more uniform, ordered, and reproducible oleate-capped SLs.

Switching from drop casting to electrospray deposition (ESD) can enable the fabrication of uniform oleate-capped SLs without macroscopic liquid flow. In ESD (also called electrohydrodynamic atomization deposition), a liquid solution or colloidal dispersion is ejected as a fine jet of charged droplets from a capillary held at a high voltage (typically 1−15 kV). These droplets then undergo Coulomb fission in flight to create a plume of much smaller droplets that deposit onto an adjacent grounded substrate.[22−24] Zeleny reported the first studies of electrospray in 1914−1917,[25−27] followed by Vonnegut and Neubauer's rediscovery of the phenomenon in 1952,[28] Taylor's explanation of the conical meniscus (Taylor cone) and jet formation in 1964,[29] and classification of the cone-jet mode and other main modes of electrospray by Cloupeau and Prunet-Foch in 1989−1990.[30−32] ESD has been used to deposit various types of colloidal microparticles[33,34]

https://doi.org/10.1021/acsnano.6c01980
ACS Nano XXXX, XXX, XXX−XXX

and nanoparticles[35−39] for over 20 years. More recently, ESD was employed to make films of colloidal QDs, including QD−polymer composites[40] and layers of CdSe/CdS/ZnS core−shell QDs for QD light-emitting diodes.[41−43] A modified version of ESD called electrohydrodynamic jet/drop printing[44,45] that utilizes a narrower nozzle, smaller nozzle-substrate distance, and lower applied voltage enabled the printing of high-resolution patterns of QDs.[46−48] There are only a few reports of ESD onto liquid surfaces, including ESD of gold and polystyrene nanoparticles onto water,[49] 500 nm polystyrene spheres onto sessile water droplets,[50] and metal salt solutions to make sheets of metal nanocrystals on water or EG.[51] To the best of our knowledge, ESD has not been used to deposit QD films on liquid surfaces or to make epi-SLs.

Here we show that ESD of decane dispersions of oleate-capped PbSe QDs onto the surface of EG produces oleate-capped SL films that are homogeneous over large areas (~20 cm^2) and have significantly less flow-induced disorder than drop-cast SL films prepared from the same QDs. ESD generates a plume of microscale droplets that gently impinge across the entire EG surface to build up a uniform and continuous layer of concentrated QD dispersion that slowly dries in place with much less macroscopic liquid flow. The combination of (i) ultrasmall droplet size, (ii) large-area, uniform, fast, and gentle deposition, and (iii) precise control of deposited volume make ESD a better choice for the fabrication of high-quality oleate-capped SL films than other nozzle-based deposition methods such as gas spraying[52−55] and inkjet printing.[56−59] Unlike the drop-cast films, the ESD films are continuous and uniform over the entire EG surface. Quantitative analysis of the straightness of the QD chains in the plane of the films shows that the ESD films have about three times lower nonlinearity (better QD positional order) than the drop-cast films. ESD makes possible the reproducible fabrication of extremely uniform, ordered, and large-area QD SLs. Epi-SLs made from electrosprayed oleate-capped SLs by photobase-triggered ligand exchange[12] show 1.5 times lower nonlinearity than drop-cast epi-SLs. The better uniformity and structural order of epi-SLs produced by ESD and photobase-driven epi-fusion make them the most promising PbX QD solids so far for observing the emergence of fully delocalized electronic states (minibands).

RESULTS AND DISCUSSION

We deposited multilayer (3D) superlattice films of oleate-capped PbSe QDs onto the surface of liquid EG using an ESD system built inside of an N_2-filled glovebox (Figure 1a,b and Methods section). ESD was performed by spraying a dispersion of PbSe QDs in decane from a metal needle biased at 5−10 kV onto a quartz Petri dish containing ~5 mm of EG. The EG was grounded by means of a circular piece of stainless steel wire cloth submerged in the liquid and connected to a high-voltage power supply via a hole drilled through the bottom of the dish. During spraying, we observed a well-formed Taylor cone-jet and vapor plume characteristic of the single cone-jet mode of ESD (Figure 1b inset).[30] The plume of charged droplets deposited preferentially on the grounded EG to form a uniform brown QD film over the entire liquid surface (Figure 1c). A representative video of the ESD process can be found in the Supporting Information (Video S1). In contrast to the ESD films, QD films made by drop casting were highly nonuniform in thickness and coverage of the EG surface for all combinations of QD concentration, liquid volume, and solvent (hexane, octane, decane) that we tested (Figure 1d and Video S2).

Characterization of stamp-transferred ESD films by scanning electron microscopy (SEM), grazing incidence small-angle X-ray scattering (GISAXS), and Fourier transform infrared (FTIR) spectroscopy revealed that the ESD films have the same SL crystal structure, ligand coverage, and optical absorption spectrum as oleate-capped SL films made by drop casting (Figure 2). SEM images showed that the films are

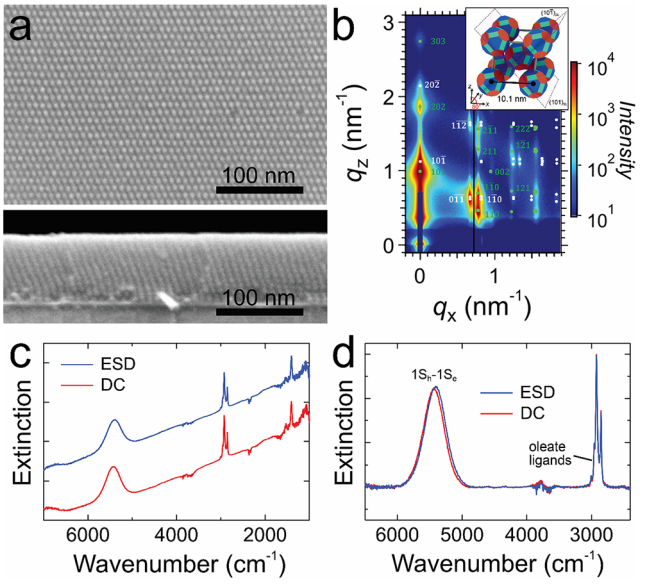

Figure 2. Characterization of ESD-made oleate-capped QD SLs. (a) Typical plan-view and cross-sectional SEM images of an ESD film transferred to a silicon substrate. The film is 80 nm thick. ESD parameters: applied bias = 8.4 kV; nozzle-to-EG distance = 8 cm; flow rate = 0.09 mL/min; QD concentration = 60 mg/mL. (b) Indexed 2D GISAXS pattern of a similarly prepared ESD film (60 nm thick). Overlaid is the calculated spot pattern for a triclinic SL ($a = c = 9.86$ nm, $b = 10.22$ nm, $\alpha = 81.2°$, $\beta = 83.3°$, $\gamma = 79.1°$) oriented with its $(101)_{SL}$ plane parallel to the substrate surface (green spots) and a second, nearly identical triclinic SL ($a = c = 9.85$ nm, $b = 10.22$ nm, $\alpha = 81.3°$, $\beta = 76.5°$, $\gamma = 79.2°$) with a $(10\bar{1})_{SL}$ in-plane orientation (white spots). For clarity, only select Miller indices are labeled. Inset is the averaged, rhombohedrally distorted bcc unit cell with the $(101)_{SL}$ and $(10\bar{1})_{SL}$ planes denoted by dashed lines. The red, blue, and cyan facets of each QD are the {100}, {111}, and {110} surfaces of PbSe, respectively. See Figure S1 for additional GISAXS data and a statistical determination of the SL unit cell parameters of these oleate-capped SLs. (c) Offset raw FTIR spectra of an ESD film and a drop-cast (DC) film. The two films are 60 ± 5 nm thick. (d) The FTIR spectra after baseline subtraction and correction for film coverage of the substrate, magnified to show the first exciton absorption peak of the QDs at ~5425 cm^{-1} (0.67 eV) and the C−H stretching peaks of the oleate ligands at 2750−3050 cm^{-1}.

highly ordered polycrystalline SLs with a distorted hexagonal arrangement of QDs in the substrate plane that is indistinguishable from the QD packing adopted by drop-cast oleate-capped SLs (Figure 2a).[11] The ESD films produced strong GISAXS spot patterns that indexed to the $(101)_{SL}$ and $(10\bar{1})_{SL}$ orientations of a body-centered unit cell with lattice parameters $a \approx b \approx c = 10.1 \pm 0.2$ nm and $\alpha \approx \beta \approx \gamma = 80 \pm 3°$ (Figure 2b). Although each individual pattern was best indexed as triclinic, on average the ESD films can be described

https://doi.org/10.1021/acsnano.6c01980
ACS Nano XXXX, XXX, XXX−XXX

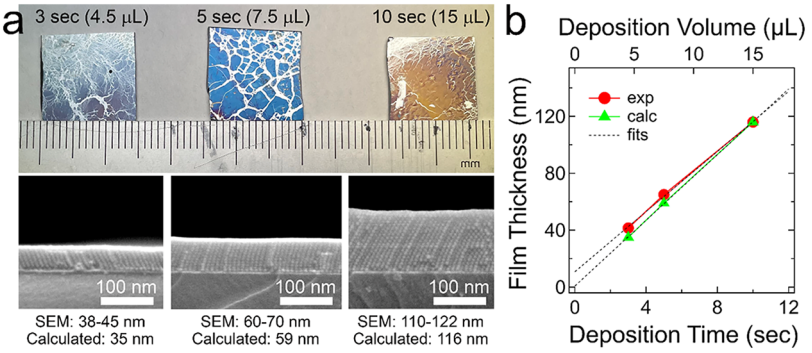

Figure 3. Facile control of ESD film thickness by changing the sprayed volume. (a) Photographs and cross-sectional SEM images of oleate-capped SL films made by spraying for 3 s (*left*), 5 s (*center*), and 10 s (*right*), followed by stamp transfer to a silicon substrate. The corresponding sprayed volumes are denoted in parentheses. The measured and calculated film thicknesses are listed below each SEM image. Calculated thicknesses assume a QD mass of 2×10^{-18} g and uniform coverage of the entire EG surface.[11] ESD parameters: 60 mg/mL, 0.09 mL/min, 8.4 kV, 8 cm nozzle-to-sample distance. (b) Plot of film thickness as a function of deposition time and volume. Dashed lines are linear fits to the data.

with a rhombohedrally distorted body centered cubic conventional unit cell (a = 10.1 nm, α = 80.0°), which is nearly identical to the SL unit cell that we reported for drop-cast films made from slightly smaller QDs.[11] Furthermore, a quantitative comparison of FTIR spectra showed that the ESD and drop-cast films have essentially the same ligand coverage and first exciton transition ($1S_h$-$1S_e$) energy and intensity (Figure 2c,d), demonstrating that ESD does not cause appreciable ligand stripping or QD size changes, structural damage, charging, or doping. Given the experimental uncertainty of the FTIR measurements, we estimate that ESD-induced charging or doping of the QDs would result in a detectable bleach of the first exciton peak only if the $1S_e$ or $1S_h$ states were occupied at a concentration greater than ~0.5 e^- per QD. Thus, the absence of a bleach means only that the QDs in the ESD films are not *highly* charged/doped. While we expect that the excess charge that accumulates in/on the QDs during ESD fully dissipates to ground to yield charge-neutral films, electrical measurements will be needed to verify this assumption by establishing whether epi-SLs made by ESD and drop casting have different electrical conductivities. The SEM, GISAXS, and FTIR data presented here demonstrate that ESD produces oleate-capped SLs with the same crystal structure as drop-cast SLs, without damaging or otherwise altering the QDs.

Several factors were identified as essential for producing uniform QD films by ESD. One important factor is the choice of solvent. We used anhydrous *n*-decane because hexane (the solvent usually used to fabricate epi-SLs by drop casting) is too volatile and tends to deposit precipitated aggregates of QDs (precipitate or powder deposition) rather than a liquid layer that slowly dries in place to yield a uniform QD film. Decane also has a very high stability limit for the QDs, is immiscible in and less dense than EG, and evaporates from the EG surface slowly enough (10–20 min) to enable high-quality QD self-assembly without unnecessarily long wait times. Decane was the shortest *n*-alkane to conveniently produce high-quality QD films.

A second consideration for making high-quality ESD films is minimizing the total sprayed volume to avoid bulk liquid flow during film drying. When the sprayed volume was too large, the liquid layer became macroscopically thick and lateral liquid flows ensued, resulting in heterogeneous ESD films that resembled drop-cast samples. We used sprayed volumes of just 5–15 μL, which form liquid layers only a few microns thick when deposited evenly across the 2-inch Petri dish. These microscopically thin liquid layers dried without significant lateral liquid flow to yield uniform QD SLs. The thickness of the QD films was tunable by changing either the QD concentration or the sprayed volume (*vide infra*).

The experimental geometry is another critical factor for achieving uniform films. We found that the electric field between the nozzle and the EG surface must be cylindrically symmetric to make uniform circular films in the circular Petri dish. Ruining this cylindrical symmetry by, for example, running the ground wire over the rim of the dish rather than through the bottom of the dish, produced asymmetric films that were thicker near the protruding grounded metal. Similarly, any insulating object placed next to the nozzle or dish accumulated surface charge during ESD, distorting the electric field and the resulting QD films. The distance between the nozzle and the EG surface was also important. Films suffered from a significant radial thickness gradient and electrohydrodynamic waves on the EG surface when the nozzle-EG distance was too short, while an excessively long distance provided no benefit but required more horizontal space in the glovebox to maintain the cylindrical symmetry of the field. We found the optimal nozzle-EG distance to be 1–2.5 times the diameter of the Petri dish.

It is also worth highlighting the importance of a deposition shutter and meniscus shield for making uniform ESD films on EG. The shutter allowed us to flush the nozzle and establish a stable cone-jet before initiating ESD on the clean EG surface. Depositions performed without a shutter typically consisted of a messy sequence of dripping (drop casting), chaotic jetting, and true ESD and produced heterogeneous films with poor thickness control. The meniscus shield—an acrylic ring placed on the dish to shield the EG-quartz meniscus from deposition (Figure 1c)—prevented pooling and pinning of the liquid layer at the meniscus and thereby improved the reproducibility of uniform films.

In addition to good lateral uniformity, ESD enabled excellent control of film thickness by adjusting the sprayed volume and/or QD concentration. Figure 3a shows photographs and cross-sectional SEM images of stamp-transferred oleate-capped SLs deposited by ESD of a 60 mg/mL dispersion for 3, 5, and 10 s, corresponding to a total sprayed volume of 4.5, 7.5, and 15 μL, respectively. Although stamping caused the films to crack, the uniform reflective color of the

https://doi.org/10.1021/acsnano.6c01980
ACS Nano XXXX, XXX, XXX−XXX

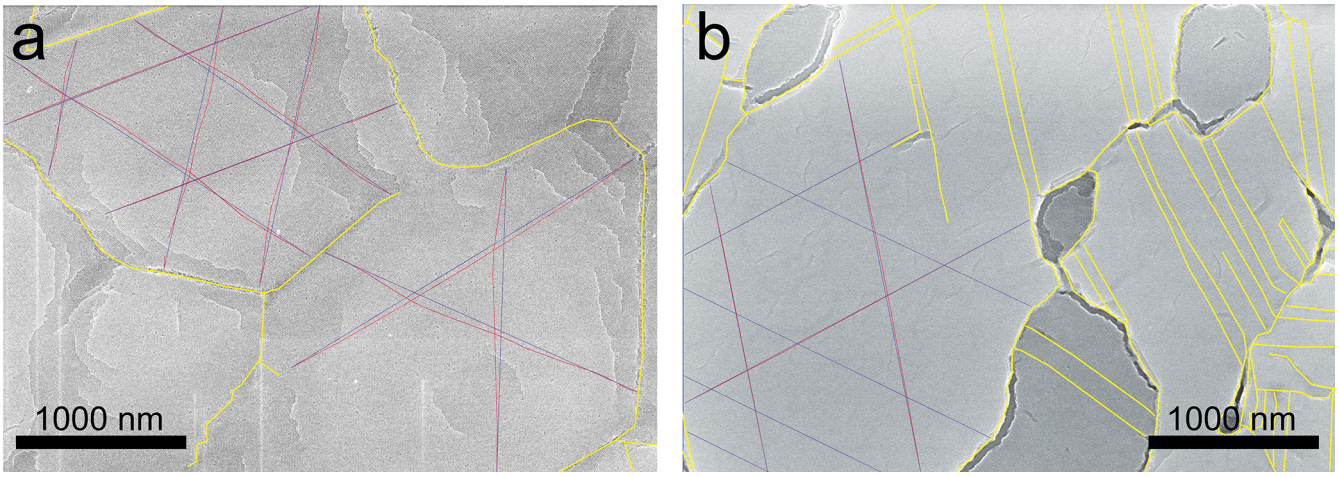

Figure 4. Comparison of the in-plane nonlinearity (meander) of QD chains in oleate-capped SL films made by drop casting versus ESD. (a) A typical high-resolution, large-area SEM image of a drop-cast film. Yellow lines denote SL grain boundaries. Red lines trace the centroids of QD chains running along one of the three principal lateral directions in the larger SL grains. Blue lines are straight line segments between the ends of each red line. The QD chains in the drop-cast film show significant nonlinearity. (b) A typical image of an ESD film. The QD chains are substantially more linear. Both films are 60 nm thick. ESD parameters: 60 mg/mL, 0.09 mL/min, 5 s, 8.4 kV, 8 cm. See Figures S4 and S5 for all images used for the nonlinearity analysis of the oleate-capped SLs.

coated areas suggests that each film has a uniform thickness, which SEM measurements at several locations on each sample confirmed. There is a linear dependence of film thickness on the spray time/volume (Figure 3b). The measured film thicknesses of 38−45 nm, 60−70 nm, and 110−122 nm, respectively, are in reasonable agreement with the expected thicknesses calculated from the total mass of QDs in each sprayed volume and the known dimensions and in-plane orientation of the SL unit cell. We have used ESD to fabricate oleate-capped SL films as thick as 250−320 nm (Figure S2) and expect that even thicker films (>1 μm) can be produced with this approach. In general, the variation in average thickness between films is ∼5% of the target thickness, while the thickness variation within individual films is typically better than 10%, as shown by atomic force microscopy (AFM), cross-sectional SEM imaging at different locations of each film, a macroscopically uniform reflective color, and optical reflectance microscopy (again looking at film color). The ability to make uniform oleate-capped SL films of controlled thickness is itself an important advance in the fabrication of epi-SLs for fundamental studies and device applications.

Submonolayer, monolayer, and bilayer films of oleate-capped QDs were also produced using ESD by spraying suitably diluted QD dispersions onto EG and stamping the floating films onto silicon substrates (Figure S3). The submonolayer films consist of isolated, roughly circular islands of QDs that are one QD thick. The monolayer samples feature mostly monolayer regions with some bare regions and some bilayer regions, while the bilayer samples contain a fraction of bare, monolayer, and trilayer regions in addition to the intended bilayer regions. These results show that ESD can be used to make well-controlled QD monolayers and bilayers over large substrate areas.

Now we evaluate whether ESD suppresses the lateral flow patterns—the riverlike meanders, arcs, and swirls of the QD chains thought to arise from macroscopic liquid flow during film drying—that are usually pronounced in drop-cast films. We reasoned that if ESD could make a sufficiently uniform and thin liquid layer, then this layer would dry in place without lateral flows and thereby reduce the flow-induced QD positional disorder in the resulting SL film. A qualitative comparison of SEM images of ESD and drop-cast films suggested that the QD chains are indeed straighter and less meandering in ESD films. We performed a quantitative statistical analysis of the degree of lateral nonlinearity of the QD chains in the two types of films using high-resolution, large-area SEM images (Figure 4, Figures S4−S5, and Table 1). First, the grain boundaries in each image were mapped (yellow lines in Figure 4) to locate large SL grains (1.5−3 μm diameter) for study. Lines were then manually drawn along the centroids of QD chains running along the three principal in-plane lattice directions in the large SL grains (red lines in Figure 4). These lines were generally curved/undulating rather than straight. Perfectly straight lines were also drawn between the two end points of each of the traced QD chains (blue lines in Figure 4). The area between each pair of red and blue lines is thus a measure of the nonlinearity of that QD chain. We define a unitless structural nonlinearity parameter $\omega = \frac{\sum_n A_n}{d \sum_n l_n}$, where A_n is the area inscribed by the nth QD chain (red lines) and the straight line segment between its two end points (blue lines), l_n is the length of the straight line segment of the nth QD chain, and d is the QD diameter. Measurement of 146 QD chains from 10 different films yielded ω = 0.51 for ESD films and ω = 1.7 for drop-cast films (Table 1). The ESD films have about three times lower nonlinearity (better QD positional order) according to this metric.

Table 1. Nonlinearity Analysis of ESD and Drop-Cast Films

	drop-cast films		ESD films	
	oleate-SL	epi-SL	oleate-SL	epi-SL
# of QD chains	65	62	81	69
average length (μm)	1.5	1.6	1.8	1.5
total length (μm)	98	101	146	103
total area (μm^2)	1.14	0.99	0.54	0.70
nonlinearity (ω)	**1.7**	**1.5**	**0.51**	**1.0**

https://doi.org/10.1021/acsnano.6c01980
ACS Nano XXXX, XXX, XXX−XXX

To determine if the superior positional order of the ESD films is retained when the oleate-capped SLs are converted to epi-SLs, we used photochemically triggered ligand exchange[12] to make epi-SLs from the floating ESD films (Figure 5 and

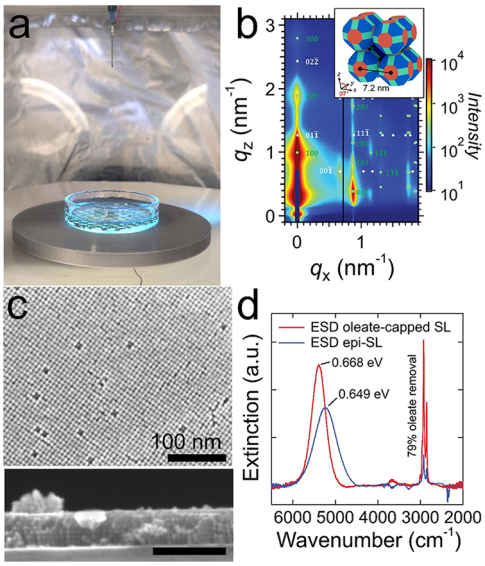

Figure 5. Epi-SL films made from ESD films. (a) Photograph of the setup during in situ photobase-triggered epi-fusion of the floating ESD film. The quartz dish is illuminated from below by an ultraviolet lamp (254 nm). Blue light is also emitted by the lamp. (b) Indexed GISAXS pattern of one of the resulting epi-SL films on a silicon substrate. The inset shows the averaged epi-SL unit cell derived from the GISAXS data. The red, blue, and cyan facets are the {100}, {111}, and {110} surfaces of PbSe, respectively. The photobase generator concentration was 1 mM; UV illumination time = 1 h; dark ligand exchange time = 2 h. (c) Typical plan-view and cross-sectional SEM images of an epi-SL film on a silicon substrate. The film is 60 nm thick. (d) FTIR spectra of an ESD epi-SL film and an ESD oleate-capped SL film after baseline subtraction and correction for film coverage of the substrate. Conversion to the epi-SL resulted in 79% oleate loss and redshifting and broadening of the first exciton peak. Both films are 60 ± 5 nm thick.

Methods section). In this process, the photobase generator (*E*)-1-piperidino-3-(2-hydroxyphenyl)-2-propen-1-one was predissolved in the EG, onto which the oleate-capped SL film was formed by ESD. The quartz dish was then illuminated from underneath by 254 nm light to photodissociate the photobase generator into coumarin and piperidine, the latter of which deprotonates EG to form glycoxide, triggering glycoxide-oleate ligand exchange and epitaxial fusion of the QDs to yield the epi-SL, as reported previously.[12] Figure 5a shows the experimental setup used for in situ photobase-triggered epi-fusion of the floating ESD films. Characterization of the stamp-transferred films by GISAXS and SEM proved that photobase-made ESD films yield the normal epi-SL structure. GISAXS spot patterns indexed well to the (100) and (01$\bar{1}$) in-plane orientations of a rhombohedrally distorted simple cubic SL with lattice constants a = 7.2 nm and α = 97°, very similar to our previous results (Figure 5b).[11] SEM images showed the films had the usual epi-SL morphology (Figure 5c). According to FTIR spectra, conversion to the epi-SL resulted in a 70−80% reduction of the oleate content of the films as well as substantial redshifting and broadening of the $1S_h$-$1S_e$ transition (by ∼20 meV and ∼15 meV, respectively; Figure 5d), which is again consistent with previous reports.[11] These results show that ESD films can be readily converted to epi-SLs using established approaches.

Nonlinearity parameters were determined for epi-SLs made from both ESD and drop-cast films. Figure 6 shows two of the 23 SEM images of epi-SLs used in our analysis. Measurement of 131 QD chains from 8 different films yielded ω = 1.0 for ESD epi-SLs and ω = 1.5 for drop-cast epi-SLs (Table 1). The ESD films have 1.5 times lower nonlinearity than the drop-cast films. Although the ω_{DC}/ω_{ESD} ratio decreased somewhat from the oleate-capped SLs to the epi-SLs, it is clear that ESD produces epi-SLs with less meander and better long-range positional order. Moreover, the X-ray scattering correlation length (ξ) determined from in-plane line cuts of the $(001)_{SL}$ peaks of the GISAXS data was also significantly longer in the ESD epi-SLs (ξ = 198−214 nm) than in the DC epi-SLs (ξ = 108−173 nm), suggesting some combination of better intragrain QD positional order—consistent with the meander analysis presented here—and larger average SL grain size in the ESD films (Figure S8). The concentration of intragrain extended defects in the ESD and DC epi-SLs was similar for films of equal oleate content (Figure S9). Superior QD positional order, film uniformity, and thickness control make ESD a much better method than drop casting for producing high-quality epi-SLs.

This study focused on ESD of PbSe QDs on a liquid surface, but ESD can undoubtedly be used to make a wide range of nanoparticle films on both liquid and solid substrates.[35−43,49,51] In addition to PbSe QD films, we also made high-quality ESD films of oleate-capped CdSe QDs[60] and $ZnFe_2O_4$ nanocrystals on EG (Figure S10). ESD is a general, powerful, and accessible method for fabricating colloidal thin films and its use will likely increase as its advantages become more widely known.

CONCLUSION

We demonstrated that electrospray deposition is a superior alternative to drop casting for producing large-area, uniform, and highly ordered PbSe QD epi-SL films. ESD minimizes lateral liquid flows during film formation and thereby decreases the medium- and long-range positional disorder of the QDs. ESD also enables precise control of film thickness over large substrate areas. Epi-SLs made from ESD films have less nonlinearity than epi-SLs made by drop casting. Future work will focus on charge transport measurements of ESD-made epi-SLs, which we anticipate possess the necessary spatial order and electronic coupling to show delocalized states and miniband transport. ESD is a powerful method for making high-quality nanoparticle films of controlled thickness for fundamental studies and applications in optoelectronics, energy conversion and storage, catalysis, and other fields.

METHODS

Materials

All chemicals were used as received unless otherwise noted. Lead oxide (PbO, 99.999%), selenium shot (99.999%), methoxytrimethylsilane (MTMS, >97%), and zinc nitrate hexahydrate (99%) were purchased from Alfa Aesar. Oleic acid (OA, technical grade, 90%), diphenylphosphine (DPP, 98%), 1-octadecene (ODE, 90%), anhydrous ethylene glycol (EG, 99.8%), anhydrous acetonitrile (99.99%), anhydrous hexanes (99%), anhydrous decane (99%), anhydrous toluene (99.8%), 3-mercaptopropyltrimethoxysilane (3-MPTMS, 95%), anhydrous isopropyl alcohol (IPA, 99.8%),

https://doi.org/10.1021/acsnano.6c01980
ACS Nano XXXX, XXX, XXX−XXX

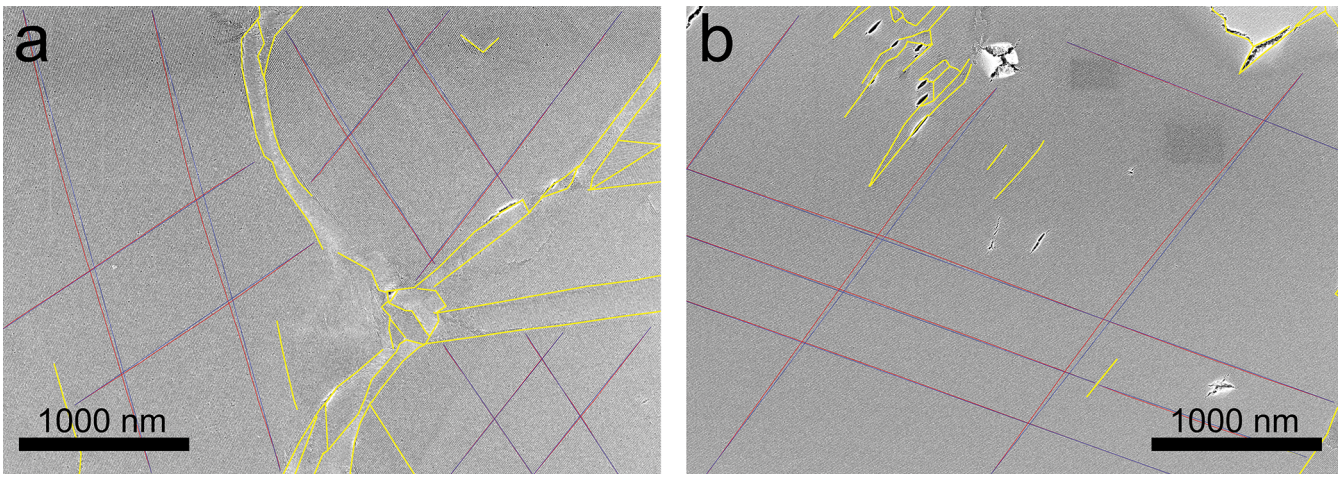

Figure 6. Comparison of the in-plane nonlinearity of QD chains in epi-SL films made by drop casting versus ESD. (a) Low-magnification, high-resolution SEM image of a drop-cast film after photobase-triggered epi-fusion. Yellow lines denote SL grain boundaries. Red lines trace the centroids of QD chains running along one of the two principal lateral directions in the epi-SL grains. Blue lines are straight line segments between the end points of each red line. (b) A typical image of an ESD film after photobase-triggered epi-fusion. Both films are ∼60 nm thick. ESD parameters: 60 mg/mL, 0.09 mL/min, 5 s, 8.4 kV, 8 cm. The photobase generator concentration was 1 mM; UV illumination time = 1 h; dark ligand exchange time = 2 h. See Figures S6 and S7 for all images used in the nonlinearity analysis of the epi-SLs.

anhydrous tetrachloroethylene (TCE, 99%), iron(III) nitrate nonahydrate (98%), and sodium hydroxide (97%) were purchased from Sigma-Aldrich. Sodium oleate (>97%) was purchased from TCI. (*E*)-1-piperidino-3-(2-hydroxyphenyl)-2-propen-1-one (WPBG-027) was purchased from Fujifilm. Tri-*n*-octylphosphine (TOP, technical grade, >97%) was acquired from Strem Chemicals and stirred with selenium shot overnight to make a colorless 1 M TOP-Se stock solution. All glassware and quartzware used for experiments were rinsed with hexane, IPA, and then deionized water, soaked overnight in a 1.5 M KOH (>85%, Acros) base bath, rinsed twice with 18.2 MΩ·cm water (Milli-Q Gradient), and thoroughly dried in a glassware oven. Double-side polished (DSP) intrinsic float-zone silicon wafers and single-side polished (SSP) degenerately doped silicon wafers were purchased from University Wafer.

PbSe Quantum Dot Synthesis

PbSe QDs were synthesized and purified using standard Schlenk line and glovebox techniques. PbO (1.50 g), OA (5.00 g), and ODE (10.00 g) were mixed in a 50 mL three-neck round-bottom flask and degassed under vacuum at room temperature. The mixture was then heated to 120 °C under vacuum to form lead oleate ($Pb(OA)_2$) and dry the solution. After 2 h at 120 °C, the colorless $Pb(OA)_2$ solution was heated to 180 °C in 30 min under argon flow and 9.6 mL of a 1 M solution of TOP-Se containing 0.2 mL of DPP was rapidly injected into the hot solution, causing an immediate and progressive darkening of the solution. After 100 s, the flask was dunked into a liquid nitrogen bath and diluted by injecting 10 mL of anhydrous toluene to terminate QD growth and ripening. The QDs were purified in an N_2-filled glovebox (<1 ppm of O_2) by adding 10 mL of acetonitrile to every 15 mL of reaction solution, collecting the QDs by centrifugation, discarding the supernatant, performing ten cycles of redispersion/precipitation using toluene/acetonitrile (5 mL/20 mL), and then drying and storing the QDs as a powder in the glovebox.

Synthesis of CdSe QDs and $ZnFe_2O_4$ Nanocrystals

5.5 nm oleate-capped CdSe QDs were synthesized according to ref 60 and provided by T. Krauss.

Zinc ferrite ($ZnFe_2O_4$) nanocrystals were synthesized using a hydrothermal reaction carried out in a Parr Model 4744 acid digestion vessel. 1.68 mmol of $Zn(NO_3)_2{\cdot}6H_2O$ and 3.36 mmol of $Fe(NO_3)_3{\cdot}9H_2O$ were added to 30 mL of water and stirred until a clear orange solution was obtained. The pH of the solution was increased to 11 by adding NaOH pellets. The solution was stirred for an additional 20 min to ensure that the pH was stable and then transferred to the Teflon cup of the stainless steel digestion vessel. The loaded and sealed digestion vessel was heated to 180 °C at a ramp rate of 5 °C/min, maintained at 180 °C for 1 h, and then cooled naturally to room temperature. The as-made red precipitate of $ZnFe_2O_4$ nanocrystals was purified by three cycles of rinsing in a 1:1 v:v mixture of water and ethanol and centrifugation at 4400 rpm for 10 min. The purified nanocrystals were then resuspended in 20 mL of water.

Biphasic ligand exchange with oleic acid was used to transfer the $ZnFe_2O_4$ nanocrystals into decane for ESD. The 20 mL aqueous dispersion of washed nanocrystals was added to a stoppered Erlenmeyer flask and stirred vigorously. Thirty mL of a 20 mM solution of oleic acid in hexane was then added to form a biphasic mixture, which was heated to 60 °C and stirred for 2 h. During this treatment, the nanocrystals moved into the upper hexane phase, while the lower aqueous phase became clear and colorless. The hexane phase was then collected using a separatory funnel. The oleate-capped $ZnFe_2O_4$ nanocrystals were then precipitated with 30 mL of ethanol, collected by centrifugation (4400 rpm for 15 min), dried overnight, weighed, and redispersed in decane to prepare a 35 mg mL^{-1} bright red dispersion for ESD. The phase purity of the nanocrystals was confirmed by powder X-ray diffraction (Rigaku SmartLab). Nanocrystal size and shape were determined by SEM and transmission electron microscopy (JEOL JEM-2800).

Electrospray Deposition of PbSe Quantum Dot Films

Electrospray deposition (ESD) of oleate-capped PbSe QD superlattice films was accomplished with a homemade ESD system built inside of a glovebox. The ESD system consists of a plexiglass enclosure, a high-voltage power supply, a syringe and needle (the ESD nozzle) mounted to a syringe pump on top of the enclosure, a rectangular plastic deposition shutter, a grounded quartz Petri dish (2 in. OD, Technical Glass Products) with an inverted UV lamp (UVGL-58, UVP) mounted on a lab jack inside the enclosure, and two removable cameras (see Figure 1). The electric field for ESD was generated by a power supply (EH60N1.5, Glassman High Voltage) with its high voltage output wired to the nozzle (a 22-gauge blunt needle, OD = 0.74 mm, ID = 0.43 mm, length = 1 in., SANANTS). A 24-gauge 316 stainless steel wire (TEMCo Industrial) was tightly wrapped around the nozzle, soldered in place, and then connected to the lead of the power supply. The needle was attached to a polypropylene syringe (1 mL, Henke-Ject), filled with the QD dispersion, and mounted directly onto the syringe pump (Legato 210, KD Scientific). A circular piece of 304 stainless steel wire cloth (74% void space, Valchoose) covering the bottom of the EG-filled Petri dish and connected to the ground stud of the power supply via a 1 mm

https://doi.org/10.1021/acsnano.6c01980
ACS Nano XXXX, XXX, XXX−XXX

hole drilled through the dish and sealed with epoxy (Torr Seal, Agilent) served as the ground electrode. The shutter was used to protect the EG surface from unwanted deposition during nozzle flushing (cleaning) and the time required to form a stable ESD cone-jet and plume. The lab jack was used to control the distance between the nozzle and the ground electrode. Typical deposition conditions were as follows: nozzle-EG distance = 6−12 cm; applied voltage = 5−10 kV; QD concentration = 60 mg/mL; flow rate = 0.05−0.1 mL/min; deposition time = 3−10 s.

ESD of QD superlattice films was accomplished by adding 10 mL of EG to the Petri dish, closing the shutter, loading the QD/decane dispersion (typically 60 mg/mL) into the syringe, flushing the nozzle at a flow rate of 0.1 mL/min for 10 s, setting the desired flow rate for ESD, activating the power supply and obtaining a stable cone-jet and plume (which typically required <10 s), and then opening the shutter to deposit the QD dispersion onto the EG surface for a designated time. The deposition was halted by stopping the syringe pump and quickly zeroing the applied voltage. In cases when a plastic meniscus shield was used to prevent deposition near the inner rim of the Petri dish, the shield was removed immediately after film deposition. The film then dried over the course of 5−30 min, yielding a brown, highly reflective, oleate-capped QD superlattice floating on the EG surface. The dried film was manually stamp transferred onto a silicon substrate using a vacuum pen. The stamped film was rinsed vigorously with neat acetonitrile and dried under nitrogen flow in the glovebox. Prior to use, the silicon substrates were cleaned in oxygen plasma (Zepto plasma cleaner, Diener Electronic), soaked in a 100 mM solution of either 3-MPTMS in toluene or MTMS in ethanol for at least 1 h inside the glovebox to functionalize their surface for improved stamping of the QD films. The substrates were subsequently rinsed with neat toluene or ethanol, respectively, and dried under flowing nitrogen before stamp transfer.

Electrospray Deposition of CdSe QD and $ZnFe_2O_4$ NC films

Films of 5.5 nm oleate-capped CdSe QDs and 5−15 nm oleate-capped $ZnFe_2O_4$ nanocrystals were deposited by ESD from decane dispersions using a procedure similar to that for PbSe QD films. Deposition conditions for the CdSe QDs NCs: nozzle-EG distance = 8 cm; applied voltage = 5−9 kV; QD concentration = 10−160 mg/mL; flow rate = 0.05−0.1 mL/min; deposition time = 3−10 s. Deposition conditions for the $ZnFe_2O_4$ NCs: nozzle-EG distance = 8.5 cm; applied voltage = 4.8 kV; NC concentration = 35 mg/mL; flow rate = 0.09 mL/min; deposition time = 15 s.

Drop Casting

Drop-cast PbSe QD films were made by pipetting 90 μL of a 10 mg/mL QD/hexane dispersion onto the EG surface (10 mL of EG in the Petri dish). The dispersion was dispensed as 4−5 droplets distributed across the dish to completely cover the EG surface. The Petri dish was then carefully covered with a glass lid fitted with an O-ring to slow the drying of the QD film. Once the film was dry (10−15 min), the lid was carefully removed and the film stamp transferred as described in the previous section.

Photobase-Triggered Conversion of Oleate-Capped Superlattices to Epitaxially Fused Superlattices

PbSe QD epi-SLs were made from oleate-capped films produced by ESD onto EG that contained 1 mM of the photobase generator WPBG-027. The ESD procedure was otherwise the same as described above. Once the QD film was completely dry, the entire Petri dish was illuminated from underneath by the UV lamp (254 nm, ~1.5 mW/cm^2 at the film position) for 1 h, after which the film remained on the EG for an additional 2 h in the dark to promote oleate removal and epi-fusion before it was stamped onto a silicon substrate, rinsed thoroughly with neat acetonitrile, and dried under flowing nitrogen.

Film Characterization

Scanning electron microscopy was performed with an FEI Magellan 400L XHR SEM operating in magnetic immersion mode (TLD detector) at 10 kV and 50−100 pA at a working distance of 4.0 mm and without beam deceleration. FTIR extinction spectra of QD films deposited on 500 μm thick, double-side-polished, intrinsic float zone Si substrates were acquired in dry air at room temperature on a Nicolet 6700 FTIR spectrometer using an XT-KBr beamsplitter and a TE-cooled DLaTGS detector. The substrate was aligned perpendicular to the beam (transmission mode). Spectra were collected at a resolution of 4 cm^{-1} using 32 scans acquired at 0.26 scans/sec. A clean Si substrate was used as the background. The spectra were baseline corrected across the C−H stretching region to enable accurate determination of oleate removal[12] by fitting each baseline using a spline function in Igor Pro and then subtracting the baseline from the raw spectrum to yield the corrected spectrum. The spline function was tailored to each spectrum to produce a flat baseline in the region of interest. Spline points were selected in featureless regions of the spectra (~5000−4000 and ~2600−2000 cm^{-1}). No smoothing functions or additional spectral manipulations were employed. SEM and FTIR data were collected on the same day the sample was prepared. Atomic force microscopy (AFM) topography imaging was performed using an Asylum Research MFP-3D AFM operating in tapping mode. Grazing-incidence small-angle X-ray scattering (GISAXS) measurements were performed on Beamline 7.3.3 of the Advanced Light Source at Lawrence Berkeley National Laboratory using 10 keV monochromatic X-rays (λ = 1.24 Å) with an energy bandwidth of 1%. The SL films were prepared on Si substrates and transported under nitrogen to minimize air exposure prior to measurement, but measurements were performed in air. A Dectris Pilatus 2 M detector with a pixel size of 0.172 × 0.172 mm and 1475 × 1679 pixels was used to record the 2D scattering patterns. A silver behenate standard was used to determine the sample-to-detector distance (2994.78 mm) and beam center. Exposure times ranged from 2 to 30 s. The incidence angle varied from 0.05° to 0.25°. Manual pattern fitting was performed using the IndexGIXS software package provided by Detlef Smilgies of the Cornell High Energy Synchrotron Source (CHESS). The critical angles of the films were fitted empirically (0.19−0.21°) to capture the breadth of the Yoneda band.

SEM Image Analysis for Nonlinearity Quantification

A series of high-resolution SEM images was acquired at 50,000× magnification (providing a field of view of 4.14 μm × 2.79 μm) at randomly selected locations of oleate-capped SL films and epi-SL films made by ESD and drop casting. For each of the four film types, 4−5 independently prepared films made with different batches of QDs on different days were imaged. All SL grain boundaries visible in each image were manually labeled with yellow lines in Adobe Photoshop. Only grains with a long dimension of 1.5−3 μm were selected for nonlinearity analysis. Smaller grains were excluded from analysis because they tended to be disordered by their nearby grain boundaries. The centroids of 2−8 QD chains running along the three principal in-plane lattice directions in each large grain were carefully manually traced with red lines (generally not straight). Straight blue lines were then drawn between the ends of each red line. The total area enclosed by each pair of red and blue lines was calculated in ImageJ, divided by the length of each blue line, and divided again by the QD diameter to arrive at a dimensionless measure of the nonlinearity of each QD chain. Statistics for oleate-capped SLs were compiled using 81 QD chains in ESD films and 65 chains in drop-cast films. For the epi-SLs, 69 QD chains in ESD films and 62 chains in drop-cast films were used to generate the reported statistics. QD chains were selected for maximum length while also ensuring a large distance between analyzed chains, roughly equal representation of chains running in each of the three hexagonal lattice directions, and sufficient image resolution to unambiguously determine the QD positions along the entire length of each QD chain. Two analysts evaluated the images. Every effort was made to avoid sampling bias and no data contrary to the working hypothesis was excluded. Several regions of severe meandering in the drop-cast films were excluded from the analysis to arrive at a conservative comparison of nonlinearity in the ESD and drop-cast films.

https://doi.org/10.1021/acsnano.6c01980
ACS Nano XXXX, XXX, XXX−XXX

■ ASSOCIATED CONTENT

Supporting Information

The Supporting Information is available free of charge at https://pubs.acs.org/doi/10.1021/acsnano.6c01980.

Lattice constants of oleate-capped SLs and epi-SLs derived from additional GISAXS patterns, SEM images of submonolayer, monolayer, and bilayer oleate-capped SL films, all SEM images used for nonlinearity analysis of the oleate-capped SL and epi-SL films, tabulated data from the nonlinearity analysis, correlation lengths determined from GISAXS patterns of ESD and DC epi-SL films, the concentration of intragrain extended defects in the different films, and results for ESD of CdSe QD and $ZnFe_2O_4$ NC films (PDF)

A representative plan-view video of the ESD deposition of a PbSe QD dispersion in decane onto the EG surface (MP4)

A representative plan-view video of drop casting a PbSe QD dispersion in hexane onto the EG surface (MP4)

Close-up video of the nozzle during 0.05 mL min^{-1} flow of a 60 mg mL^{-1} dispersion of PbSe QDs in decane (applied bias = 8.4 kV) (MP4)

Close-up video of the nozzle during 0.05 mL min^{-1} flow of a 60 mg mL^{-1} dispersion of PbSe QDs in decane (applied bias = 0 kV) (MP4)

Close-up video of the nozzle during 0.05 mL min^{-1} flow of pure decane (applied bias = 8.4 kV) (MP4)

Close-up video of the nozzle during 0.05 mL min^{-1} flow of pure decane (applied bias = 0 kV) (MP4)

High-resolution TEM images for Figures S3−S7 (ZIP)

■ AUTHOR INFORMATION

Corresponding Author

Matt Law − *Department of Chemistry, University of California, Irvine, Irvine, California 92697, United States; Department of Materials Science and Engineering, University of California, Irvine, Irvine, California 92697, United States; Department of Chemical and Biomolecular Engineering, University of California, Irvine, Irvine, California 92697, United States;* orcid.org/0000-0001-7645-9908; Email: matt.law@uci.edu

Authors

Geemin Kim − *Department of Materials Science and Engineering, University of California, Irvine, Irvine, California 92697, United States*

Cristian Reynaga Gonzalez − *Department of Physics and Astronomy, University of California, Irvine, Irvine, California 92697, United States*

Complete contact information is available at: https://pubs.acs.org/10.1021/acsnano.6c01980

Author Contributions

G.K. performed the experiments. C.R.G. assisted G.K. with ESD, performed AFM measurements, and synthesized the $ZnFe_2O_4$ nanocrystals. M.L. directed the study and contributed to data interpretation. M.L. wrote the manuscript with input from all authors.

Notes

The authors declare no competing financial interest.

■ ACKNOWLEDGMENTS

This work was supported by the U.S. Department of Energy (DOE), Office of Science, Office of Basic Energy Sciences, Materials Chemistry Program under Award Number DE-SC0024658. The authors acknowledge the use of facilities and instrumentation at the UC Irvine Materials Research Institute (IMRI), which is supported in part by the National Science Foundation through the UC Irvine Materials Research Science and Engineering Center (DMR-2011967). This research used Beamline 7.3.3 of the Advanced Light Source, a U.S. DOE Office of Science User Facility under contract no. DE-AC02-05CH11231. The authors thank C. McCormick for assistance in building the electrospray deposition setup, E. Schaible and R. Li for support with GISAXS experiments, D. Smilgies for advice on indexing GISAXS patterns, T. Krauss for providing CdSe QDs, J. Ragadi and L. Brennan for assistance with XRD, and H. Ruffo for TEM imaging of the $ZnFe_2O_4$ NCs.

■ REFERENCES

(1) Deveaud, B.; Shah, J.; Damen, T. C.; Lambert, B.; Regreny, A. Bloch transport of electrons and holes in superlattice minibands: direct measurement by subpicosecond luminescence spectroscopy. *Phys. Rev. Lett.* **1987**, *58*, 2582−2585.

(2) Remacle, F.; Levine, R. D. Quantum dots as chemical building blocks: elementary theoretical considerations. *ChemPhysChem* **2001**, *2*, 20−36.

(3) Jiang, C.-W.; Green, M. A. Silicon quantum dot superlattices: Modeling of energy bands, densities of states, and mobilities for silicon tandem solar cell applications. *J. Appl. Phys.* **2006**, *99*, No. 114902.

(4) Kalesaki, E.; Evers, W. H.; Allan, G.; Vanmaekelbergh, D.; Delerue, C. Electronic structure of atomically coherent square semiconductor superlattices with dimensionality below two. *Phys. Rev. B* **2013**, *88*, No. 115431.

(5) Baumgardner, W. J.; Whitham, K.; Hanrath, T. Confined-but-connected quantum solids via controlled ligand displacement. *Nano Lett.* **2013**, *13*, 3225−3231.

(6) Evers, W. H.; Goris, B.; Bals, S.; Casavola, M.; de Graaf, J.; van Roij, R.; Dijkstra, M.; Vanmaekelbergh, D. Low-dimensional semiconductor superlattices formed by geometric control over nanocrystal attachment. *Nano Lett.* **2013**, *13*, 2317−2323.

(7) Sandeep, C. S. S.; Azpiroz, J. M.; Evers, W. H.; Boehme, S. C.; Moreels, I.; Kinge, S.; Siebbeles, L. D. A.; Infante, I.; Houtepen, A. J. Epitaxially connected PbSe quantum-dot films: controlled neck formation and optoelectronic properties. *ACS Nano* **2014**, *8*, 11499−11511.

(8) Kalesaki, E.; Delerue, C.; Morais Smith, C.; Beugeling, W.; Allan, G.; Vanmaekelbergh, D. Dirac cones, topological edge states, and nontrivial flat bands in two-dimensional semiconductors with a honeycomb nanogeometry. *Phys. Rev. X* **2014**, *4*, No. 011010.

(9) Whitham, K.; Yang, J.; Savitzky, B. H.; Kourkoutis, L. F.; Wise, F.; Hanrath, T. Charge transport and localization in atomically coherent quantum dot solids. *Nat. Mater.* **2016**, *15*, 557−563.

(10) Gómez-Campos, F. M.; Rodríguez-Bolívar, S.; Califano, M. High-mobility toolkit for quantum dot films. *ACS Photonics* **2016**, *3*, 2059−2067.

(11) Abelson, A.; Qian, C.; Salk, T.; Luan, Z.; Fu, K.; Zheng, J.-G.; Wardini, J. L.; Law, M. Collective topo-epitaxy in the self-assembly of a 3D quantum dot superlattice. *Nat. Mater.* **2020**, *19*, 49−55.

(12) Qian, C.; Abelson, A.; Miller-Casas, A.; Capp, R.; Vinogradov, I.; Udagawa, N. S.; Ge, N.-H.; Law, M. Photobase-triggered formation of 3D epitaxially fused quantum dot superlattices with high uniformity and low bulk defect densities. *ACS Nano* **2022**, *16*, 3239−3250.

(13) Abelson, A.; Qian, C.; Crawford, Z.; Zimanyi, G. T.; Law, M. High-mobility hole transport in single-grain PbSe quantum dot superlattice transistors. *Nano Lett.* **2022**, *22*, 9578−9585.

(14) Dong, A.; Chen, J.; Vora, P. M.; Kikkawa, J. M.; Murray, C. B. Binary nanocrystal superlattice membranes self-assembled at the liquid−air interface. *Nature* **2010**, *466*, 474−477.
(15) Weidman, M. C.; Smilgies, D.-M.; Tisdale, W. A. Kinetics of the self-assembly of nanocrystal superlattices measured by real-time *in situ* x-ray scattering. *Nat. Mater.* **2016**, *15*, 775−781.
(16) Boles, M. A.; Engel, M.; Talapin, D. V. Self-assembly of colloidal nanocrystals: from intricate structures to functional materials. *Chem. Rev.* **2016**, *116*, 11220−11289.
(17) Boneschanscher, M. P.; Evers, W. H.; Geuchies, J. J.; Altantzis, T.; Goris, B.; Rabouw, F. T.; van Rossum, S. A. P.; van der Zant, H. S. J.; Siebbeles, L. D. A.; Tendeloo, G. V.; Swart, I.; Hilhorst, J.; Petukhov, A. V.; Bals, S.; Vanmaekelbergh, D. Long-range orientation and atomic attachment of nanocrystals in 2D honeycomb superlattices. *Science* **2014**, *344*, 1377−1380.
(18) Balazs, D. M.; Matysiak, B. M.; Momand, J.; Shulga, A. G.; Ibanez, M.; Kovalenko, M. V.; Kooi, B. J.; Loi, M. A. Electron mobility of 24 $cm^2 V^{-1} s^{-1}$ in PbSe colloidal-quantum-dot superlattices. *Adv. Mater.* **2018**, *30*, No. 1802265.
(19) Liu, Y.; Tolentino, J.; Gibbs, M.; Ihly, R.; Perkins, C. L.; Liu, Y.; Crawford, N.; Hemminger, J. C.; Law, M. PbSe quantum dot field-effect transistors with air-stable electron mobilities above 7 $cm^2 V^{-1} s^{-1}$. *Nano Lett.* **2013**, *13*, 1578−1587.
(20) Liu, Y.; Gibbs, M.; Perkins, C. L.; Tolentino, J.; Zarghami, M. H.; Bustamante, J., Jr.; Law, M. Robust, functional nanocrystal solids by infilling with atomic layer deposition. *Nano Lett.* **2011**, *11*, 5349−5355.
(21) Tolentino, J.; Gibbs, M.; Abelson, A.; Law, M. Elimination of the bias-stress effect in ligand-free quantum dot field-effect transistors. *J. Chem. Phys.* **2023**, *159*, No. 044709.
(22) Jaworek, A.; Sobczyk, A. T. Electrospraying route to nanotechnology: An overview. *J. Electrostat.* **2008**, *66*, 197−219.
(23) Xie, J.; Jiang, J.; Davoodi, P.; Srinivasan, M. P.; Wang, C.-H. Electrohydrodynamic atomization: A two-decade effort to produce and process micro-/nanoparticulate materials. *Chem. Eng. Sci.* **2015**, *125*, 32−57.
(24) Gañán-Calvo, A. M.; López-Herrera, J. M.; Herrada, M. A.; Ramos, A.; Montanero, J. M. Review on the physics of electrospray: From electrokinetics to the operating conditions of single and coaxial Taylor cone-jets, and AC electrospray. *J. Aerosol Sci.* **2018**, *125*, 32−56.
(25) Zeleny, J. The electrical discharge from liquid points, and a hydrostatic method of measuring the electric intensity at their surfaces. *Phys. Rev.* **1914**, *3*, 69−91.
(26) Zeleny, J. On the conditions of instability of electrified drops, with applications to the electrical discharge from liquid points. *Proc. Camb. Philos. Soc.* **1915**, *18*, 71−83.
(27) Zeleny, J. Instability of electrified liquid surfaces. *Phys. Rev.* **1917**, *10*, 1−6.
(28) Vonnegut, B.; Neubauer, R. L. Production of monodisperse liquid particles by electrical atomization. *J. Colloid Sci.* **1952**, *7*, 616−622.
(29) Taylor, G. I. Disintegration of water drops in an electric field. *Proc. R. Soc. London A* **1964**, *280*, 383−397.
(30) Cloupeau, M.; Prunet-Foch, B. Electrostatic spraying of liquids in cone-jet mode. *J. Electrostat.* **1989**, *22*, 135−159.
(31) Cloupeau, M.; Prunet-Foch, B. Electrostatic spraying of liquids: Main functioning modes. *J. Electrostat.* **1990**, *25*, 165−184.
(32) Cloupeau, M.; Prunet-Foch, B. Electrohydrodynamic spraying functioning modes: A critical review. *J. Aerosol Sci.* **1994**, *25*, 1021−1036.
(33) Teng, W. D.; Huneiti, Z. A.; Machowski, W.; Evans, J. R. G.; Edirisinghe, M. J.; Balachandran, W. Towards particle-by-particle deposition of ceramics using electrostatic atomization. *J. Mater. Sci. Lett.* **1997**, *16*, 1017−1019.
(34) Balachandran, W.; Maio, P.; Xiao, P. Electrospray of fine droplets of ceramic suspensions for thin-film preparation. *J. Electrostat.* **2001**, *50*, 249−263.
(35) Schulz, F.; Franzka, S.; Schmid, G. Nanostructured surfaces by deposition of metal nanoparticles by means of spray techniques. *Adv. Funct. Mater.* **2002**, *12*, 532−536.
(36) Lenggoro, I. W.; Xia, B.; Okuyama, K.; Fernandez de la Mora, J. Sizing of colloidal nanoparticles by electrospray and differential mobility analyzer methods. *Langmuir* **2002**, *18*, 4584−4591.
(37) Jayasinghe, S. N.; Edirisinghe, M. J.; Wang, D. Z. Controlled deposition of nanoparticle clusters by electrohydrodynamic atomization. *Nanotechnology* **2004**, *15*, No. 1519.
(38) Suh, J.; Han, B.; Okuyama, K.; Choi, M. Highly charging of nanoparticles through electrospray of nanoparticle suspension. *J. Colloid Interface Sci.* **2005**, *287*, 135−140.
(39) Samarasinghe, S. R.; Pastoriza-Santos, I.; Edirisinghe, M. J.; Reece, M. J.; Liz-Marzán, L.; Nangrejo, M. R.; Ahmad, Z. Electric-jet assisted layer-by-layer deposition of gold nanoparticles to prepare conducting tracks. *Nat. Sci.* **2009**, *1*, 142−150.
(40) Hong, S. P.; Park, H.-Y.; Oh, J. H.; Yang, H.; Jang, S.-Y.; Do, Y. R. Fabrication of wafer-scale free-standing quantum dot/polymer nanohybrid films for white-light emitting diodes using an electrospray method. *J. Mater. Chem. C* **2014**, *2*, 10439−10445.
(41) Nguyen, T. C.; Can, T. T. T.; Choi, W.-S. Electrohydrodynamic jet-sprayed quantum dots for solution-processed light-emitting diodes. *Opt. Mater. Express* **2018**, *8*, No. 3738.
(42) Nguyen, T. C.; Can, T. T. T.; Choi, W. S. Optimization of quantum dot thin films using electrohydrodynamic jet spraying for solution-processed quantum dot light-emitting diodes. *Sci. Rep.* **2019**, *9*, No. 13885.
(43) Nguyen, T. C.; Choi, W.-S. Electrospray mechanism for quantum dot thin-film formation using an electrohydrodynamic jet and light-emitting device application. *Sci. Rep.* **2020**, *10*, No. 11075.
(44) Park, J.-U.; Hardy, M.; Kang, S. J.; Barton, K.; Adair, K.; Mukhopadhyay, D. K.; Lee, C. Y.; Strano, M. S.; Alleyne, A. G.; Georgiadis, J. G.; Ferreira, P. M.; Rogers, J. A. High-resolution electrohydrodynamic jet printing. *Nat. Mater.* **2007**, *6*, 782−789.
(45) Poon, H. F.; Saville, D. A.; Aksay, I. A. Linear colloidal crystal arrays by electrohydrodynamic printing. *Appl. Phys. Lett.* **2008**, *93*, No. 133114.
(46) Galliker, P.; Schneider, J.; Eghlidi, H.; Kress, S.; Sandoghdar, V.; Poulikakos, D. Direct printing of nanostructures by electrostatic autofocussing of ink nanodroplets. *Nat. Commun.* **2012**, *3*, No. 890.
(47) Kress, S. J. P.; Richner, P.; Jayanti, S. V.; Galiker, P.; Kim, D. K.; Poulikakos, D.; Norris, D. J. Near-field light design with colloidal quantum dots for photonics and plasmonics. *Nano Lett.* **2014**, *14*, 5827−5833.
(48) Kim, B. H.; Onses, M. S.; Lim, J. B.; Nam, S.; Oh, N.; Kim, H.; Yu, K. J.; Lee, J. W.; Kim, J.-W.; Kang, S.-K.; Lee, C. H.; Lee, J.; Shin, J. H.; Kim, N. H.; Leal, C.; Shim, M.; Rogers, J. A. High-resolution patterns of quantum dots formed by electrohydrodynamic jet printing for light-emitting diodes. *Nano Lett.* **2015**, *15*, 969−973.
(49) Nie, H.-L.; Dou, X.; Tang, Z.; Jang, H. D.; Huang, J. High-yield spreading of water-miscible solvents on water for Langmuir-Blodgett assembly. *J. Am. Chem. Soc.* **2015**, *137*, 10683−10688.
(50) Ghafouri, A.; Zhao, M.; Singler, T. J.; Yong, X.; Chiarot, P. R. Interfacial targeting of sessile droplets using electrospray. *Langmuir* **2018**, *34*, 7445−7454.
(51) Sarkar, D.; Singh, R.; Som, A.; Manju, C. K.; Ganayee, M. A.; Adhikari, R.; Pradeep, T. Electrohydrodynamic assembly of ambient ion-derived nanoparticles to nanosheets at liquid surfaces. *J. Phys. Chem. C* **2018**, *122*, 17777−17783.
(52) Zhu, T.; Shanmugasundaram, K.; Price, S. C.; Ruzyllo, J.; Zhang, F.; Xu, J.; Mohney, S. E.; Zhang, Q.; Wang, A. Y. Mist fabrication of light emitting diodes with colloidal nanocrystal quantum dots. *Appl. Phys. Lett.* **2008**, *92*, No. 023111.
(53) Kramer, I. J.; Moreno-Bautista, G.; Minor, J. C.; Kopilovic, D.; Sargent, E. H. Colloidal quantum dot solar cells on curved and flexible substrates. *Appl. Phys. Lett.* **2014**, *105*, No. 163902.
(54) Kramer, I. J.; Minor, J. C.; Moreno-Bautista, G.; Rollny, L.; Kanjanboos, P.; Kopilovic, D.; Thon, S. M.; Carey, G. H.; Chou, K. W.; Zhitomirsky, D.; Amassian, A.; Sargent, E. H. Efficient spray-

https://doi.org/10.1021/acsnano.6c01980
ACS Nano XXXX, XXX, XXX−XXX

coated colloidal quantum dot solar cells. *Adv. Mater.* **2015**, *27*, 116−121.
(55) Chen, W.; Tang, H.; Chen, Y.; Heger, J. E.; Li, N.; Kreuzer, L. P.; Xie, Y.; Li, D.; Anthony, C.; Pikramenou, Z.; Ng, K. W.; Sun, X. W.; Wang, K.; Müller-Buschbaum, P. Spray-deposited PbS colloidal quantum dot solid for near-infrared photodetectors. *Nano Energy* **2020**, *78*, No. 105254.
(56) Böberl, M.; Kovalenko, M. V.; Gamerith, S.; List, E. J. W.; Heiss, W. Inkjet-printed nanocrystal photodetectors operating up to 3 μm wavelengths. *Adv. Mater.* **2007**, *19*, 3574−3578.
(57) Sliz, R.; Lejay, M.; Fan, J. Z.; Choi, M.-J.; Kinge, S.; Hoogland, S.; Fabritius, T.; Pelayo García de Arquer, F.; Sargent, E. H. Stable colloidal quantum dot inks enable inkjet-printed high-sensitivity infrared photodetectors. *ACS Nano* **2019**, *13*, 11988−11995.
(58) Nayak, L.; Mohanty, S.; Nayak, S. K.; Ramadoss, A. A review on inkjet printing of nanoparticle inks for flexible electronics. *J. Mater. Chem. C* **2019**, *7*, 8771−8795.
(59) Balazs, D. M.; Erkan, N. D.; Quien, M.; Hanrath, T. Inkjet printing of epitaxially connected nanocrystal superlattices. *Nano Res.* **2022**, *15*, 4536−4543.
(60) Flamee, S.; Cirillo, M.; Abe, S.; Nolf, K. D.; Gomes, R.; Aubert, T.; Hens, Z. Fast, high yield, and high solid loading synthesis of metal selenide nanocrystals. *Chem. Mater.* **2013**, *25*, 2476−2483.

https://doi.org/10.1021/acsnano.6c01980
ACS Nano XXXX, XXX, XXX−XXX